Multilayer-Coated Micro-Grating Array for X-Ray Phase-Contrast Imaging

Susanna K. Lynch[a], Chian Liu[b], Lahsen Assoufid[b], Nicole Y. Morgan[c], Dumitru Mazilu[a], Eric Bennett[a], Camille K. Kemble[a], Han Harold Wen*[a]

[a]Laboratory of Imaging Physics, Biophysics and Biochemistry Center, National Heart, Lung and Blood Institute, National Institutes of Health, 10 Center Drive, Bethesda MD 20892-1061;
[b]Argonne National Laboratory, X-ray Science Division
9700 South Cass Avenue, Argonne, IL 60439;
[c]Intramural Research Programs, National Institute of Biomedical Imaging and Bioengineering, National Institutes of Health, 13 South Drive, Bethesda, MD 20892-5766

ABSTRACT

X-ray imaging techniques based on grating interferometers rely on transmission gratings to detect x-ray refraction and scattering in a sample. Gratings periods below 2 microns are challenging to realize due to the high aspect ratio of the structures. We propose a method to fabricate transmission gratings with sub-micron periods over centimeter areas by multilayer coating of a staircase (echelle) substrate. The advantage of this approach is the high aspect ratio of multilayer coating and the large area of the echelle substrate. The staircase pattern is etched on the surface of a silicon wafer through anisotropic etching. Multiple layers are deposited on the horizontal surfaces of the stairs by magnetron sputtering in a single run. The layers alternate between two materials of different absorption coefficients or refractive indices. The layer thickness d is designed to be (stair height)/2N, where 2N is the total number of layers. The incident x-ray beam is parallel to the layers and oblique to the wafer surface. Each stair of the echelle substrate forms a micro grating of period 2d, and the array of micro gratings together act as a single grating over a large area given the right continuity conditions. The grating period potentially can be below 100 nm. We present theoretical description of wave diffraction by the grating array, and results of the first fabrication test with magnetron sputtering deposition.

Keywords: x-ray, grating, multilayer, phase-contrast, dark-field, imaging, CT, interferometer

1. INTRODUCTION

X-ray phase sensitive imaging techniques based on grating interferometers use one or more gratings in the x-ray beam to produce a dense fringe pattern on the detector. When a sample of interest is placed into the beam, the position and amplitude of the fringes will change as a result of x-ray refraction and diffraction in the sample[1-8]. The refraction and diffraction of light reflect perturbations of the phase of the wavefront, and thus this type of techniques are "phase-sensitive". The advantages of the grating-based approach are that its sensitivity increases proportionally with the density of the gratings, and that large-area transmission gratings permit full field imaging without the need for raster or line scanning. X-ray refraction and diffraction arise from spatial variation of the refractive index in the material on different length scales. Macroscopic boundaries between different refractive indices causes refractive bending of the x-rays, resulting in shifting of the fringes on the detector. Structures that are much smaller than the fringe period do not cause visible fringe shifts, but increased angular divergence of the beam (diffraction)[9] and a drop in the amplitude of the fringes.

To illustrate the relationship between phase sensitivity and the grating period, a basic x-ray grating interferometer is shown in figure 1. A monochromatic x-ray beam illuminates a grating of period P at right angle, which diffracts it into two beams of order +1 and -1. The angle between the two diffracted beams is given by

$$\theta = 2\arcsin(\lambda / P) \approx 2\lambda / P, \quad (1)$$

where λ is the x-ray wavelength. The intensity on the image screen is given by the sum of the two diffracted beams:

$$I(x) = I_0 \left| \exp(i2\pi x / P + \varphi_+) + \exp(-i2\pi x / P + \varphi_-) \right|^2 , \\ = I_0 / 2 + I_0 \cos(4\pi x / P + \varphi_+ - \varphi_-) / 2 \quad (2)$$

where φ_+ and φ_- are phase delays experienced by the two beams from the grating to the image screen. Equation 2 shows that the intensity on the image screen contains a sinusoidal oscillation at the period of $P/2$, i.e., interference fringes. The position of the fringes is influenced by the difference $\varphi_+ - \varphi_-$. When a sample is present, in the short wavelength limit the phase φ_+ and φ_- at point x on the image plane are given by path integrals along the paths illustrated in Fig.1[10]. Given the distance L between the sample and the image screen, the phase difference is then

$$\varphi_+(x) - \varphi_-(x) = \int_{beam\ path} \frac{4\pi L}{P} \frac{\partial n}{\partial x} dl , \quad (3)$$

where n is the index of refraction in the sample. Therefore, the observed phase shift of the fringes reflects the gradient of the index of refraction in the x direction. The sensitivity of detection is proportional to the grating density $1/P$.

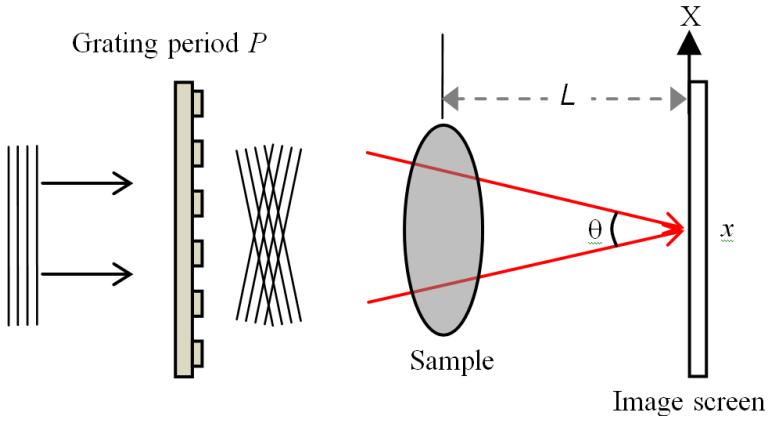

Figure 1. In this basic interferometer, an incident monochromatic x-ray beam is diffracted into two beams by a beam splitter grating. The red lines represent the directions of wave propagation of the two diffracted beams. They terminate at the point x on the image screen. In the short wavelength limit, they are the integral paths for calculating the phase of the diffracted waves at point x.

Classical x-ray transmission gratings are fabricated with photo or electron-beam lithography processes[11]. The grating typically consists of periodic vertical structures. Figure 2 shows electron micrographs of the cross-section of a silicon phase grating, which was made with reactive ion etching. The silicon walls cause a phase delay $\Delta\varphi = \delta n * h/\lambda$ relative to the trenches between the walls, where δn is the difference in refractive index between silicon and air, and h is the height of the walls. In absorption mask gratings, the trenches are filled with a metal that efficiently absorbs x-ray, such as gold. The intensity attenuation is $\exp(-\mu * h)$, where μ is the linear attenuation coefficient.

For absorption gratings, the height of the wall needs to be sufficient to modulate the transmitted intensity. So, while maintaining the height of the wall, higher phase sensitivity demands smaller grating periods and thinner walls. Thus the aspect ratio, defined as the height-to-width ratio of the walls, becomes a significant challenge in fabrication. Currently, aspect ratios beyond 20 are practically difficult to achieve in large enough areas for imaging applications. This is because the very thin walls tend to collapse during the fabrication process[12]. Grating periods below 2 microns are rare. The aspect ratio limitation has also been encountered in the fabrication of Fresnel zone plates for x-ray microscopy. There an effective solution has been to fabricate zone plates from a multilayer deposition process, where layers of alternating materials are deposited on a flat Si wafer at controlled thicknesses according to the zone-plate law[13, 14]. A multilayer Laue lens is then obtained by slicing and polishing the coated wafer. When an x-ray beam shines on the sliced and polished lens in transmission geometry, the transmitted x-rays are diffracted and focused in the same way as by a zone plate. When the thicknesses of the multilayers are uniform, the structure can act as a transmission grating for x-ray lithography [15]. Here alternating layers of Si and WSi_2 are deposited up to a total thickness of tens of microns. However,

the width of the multilayer gratings are limited to the total thickness of the multilayer stack, which does not exceed 50 microns due to inherent limits of the multilayer process.

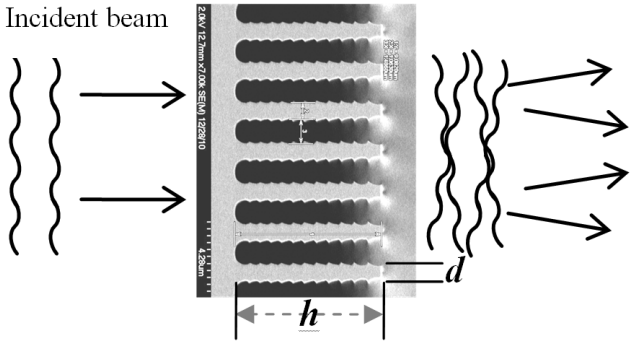

Figure 2. In this scanning electron micrograph of the cross-section of a silicon phase grating, the height of the silicon walls is *h* and the width is *d*. The aspect ratio is *h*/*d*. Ultra small grating periods are difficult to achieve in large areas due to the instability of walls of extreme aspect ratios.

In the following we propose a method to fabricate multilayer transmission gratings of large areas without the need for sectioning or stitching (Fig.3), using a design similar to multilayer-coated EUV reflective gratings[16]. The substrate surface of the grating has the shape of a staircase, and multiple layers of alternating materials are deposited on the horizontal surfaces of the stairs in a single deposition run by orienting the substrate at an angle relative to the deposition beams. The result is that each stair bears a multilayer grating of approximately 10 micron width. The whole structure is an array of such gratings. By tuning the thickness and number of layers to ensure continuity between the micro gratings, the array serves as a single grating over an extended area.

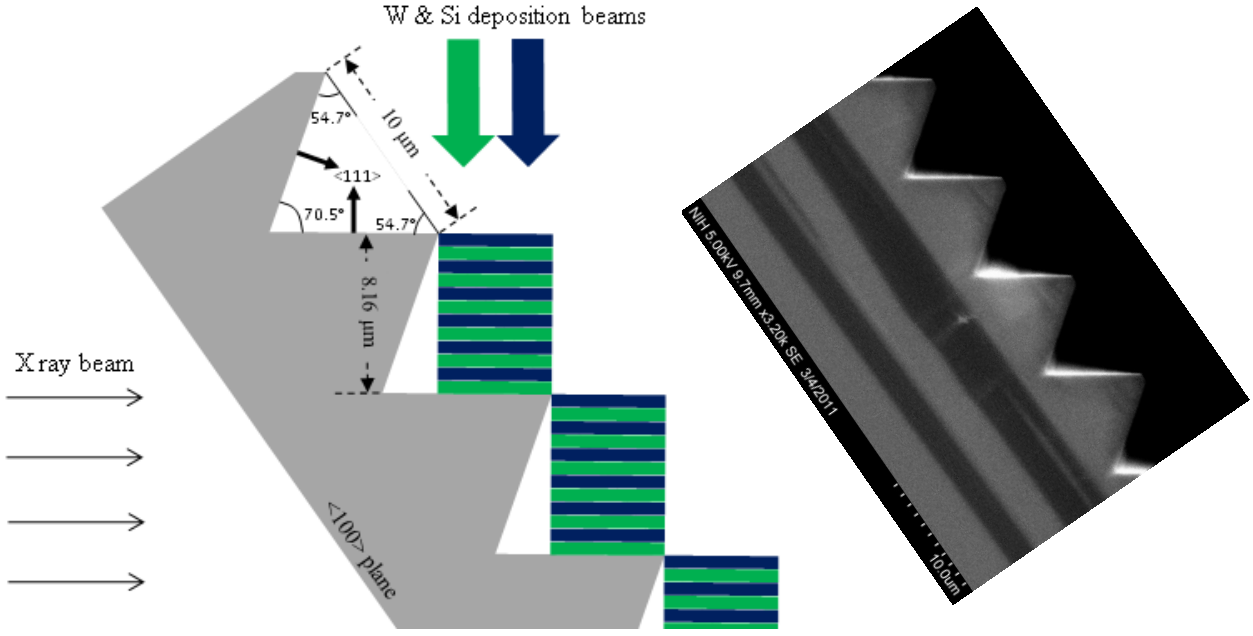

Figure 3. Left: The design parameters of the substrate and the geometry of the multilayer coating. Right: An SEM of a cleaved cross section of the silicon substrate. The dark bands are laminations from the cleaving process.

2. THEORETICAL MODELING OF WAVE DIFFRACTION

To describe wave diffraction by the grating array we use the coordinate system shown in the schematics in figure 4. The height of each stair of the substrate is H, the period of the micro-gratings is P equal to $2d$, and the angle between the floor (<111>) surfaces of the stairs and the back surface (<100>) of the wafer is α. The X axis of the coordinate system is parallel to the back surface and perpendicular to the edges of the stairs. The Z axis is perpendicular to the back surface.

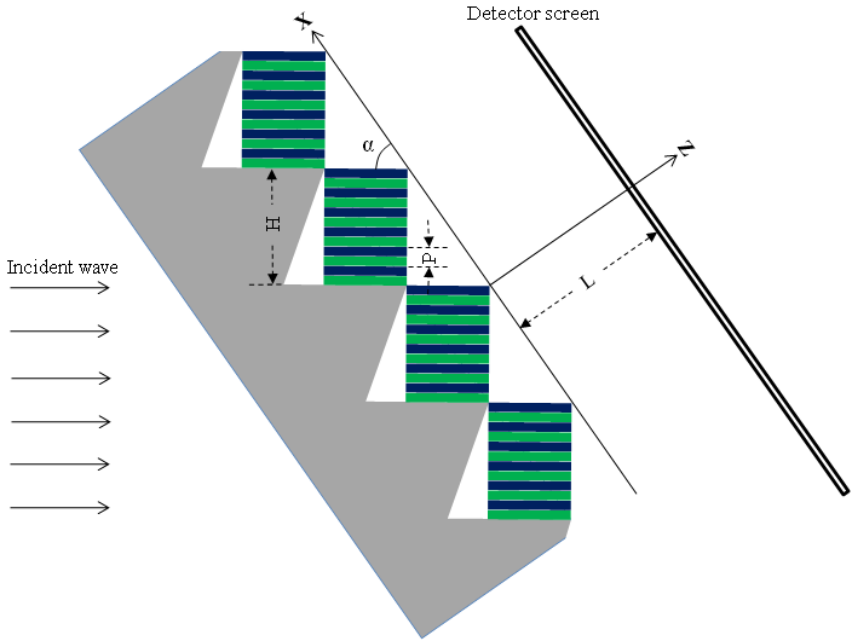

Figure 4. Theoretical description of wave diffraction by the grating array is considered in this coordinate system.

We consider the complex wave on the XY plane at z = 0. It is modulated by mask function of the grating $M(x)$ as

$$A(x, z=0) = A_0 \exp(ik_x x) M(x), \tag{4}$$

where $k_x = k\cos\alpha$, and $k = 2\pi/\lambda$. The diffraction orders correspond to the Fourier components of $M(x)$ in the X direction. To obtain the Fourier transformation of M, the grating array is regarded as a two-step modification of a continuous grating of period $P/\sin\alpha$ on the XY plane. First it is masked by a function $f(x)$ defined in a single substrate period of $H/\sin\alpha$ and describes the modulation from a single stair of the substrate. This results in the mask function of a single micro grating. Then it is convolved with a fence function of period $H/\cos\alpha$ to produce the grating array. From this view, we obtain the Fourier transformation

$$M'(k_x) = \sum_{m,n} B_m f'(2\pi n \sin\alpha / H - 2\pi m \sin\alpha / P)\delta(k_x - 2\pi m \sin\alpha / H), \tag{5}$$

where B_m are the Fourier coefficients of a multilayer grating of infinite number of layers, and f' is the Fourier transformation of $f(x)$.

It is worth noting that the single micro grating envelope function $f(x)$ expresses the truncation of an infinite multilayer grating to the height H, and additionally, a linear phase ramp across the layers due to the varying thickness of Si over a single substrate step that the x-rays pass through:

$$f(x) = f_0(x) \exp[i\delta n 2\pi x / (\lambda \sin 2\alpha)], \tag{6}$$

where δn is the difference in refractive index between silicon and air. Figure 5 is a schematic representation of the Fourier spectrum M'. It is an addition of a series of f' centered at integer multiples of $2\pi\sin\alpha / P$, and discretized by steps

of $2\pi\sin\alpha/H$. Effectively, the substrate and the repeating array introduce fine structures to the diffraction orders of an ideal, continuous multilayer grating.

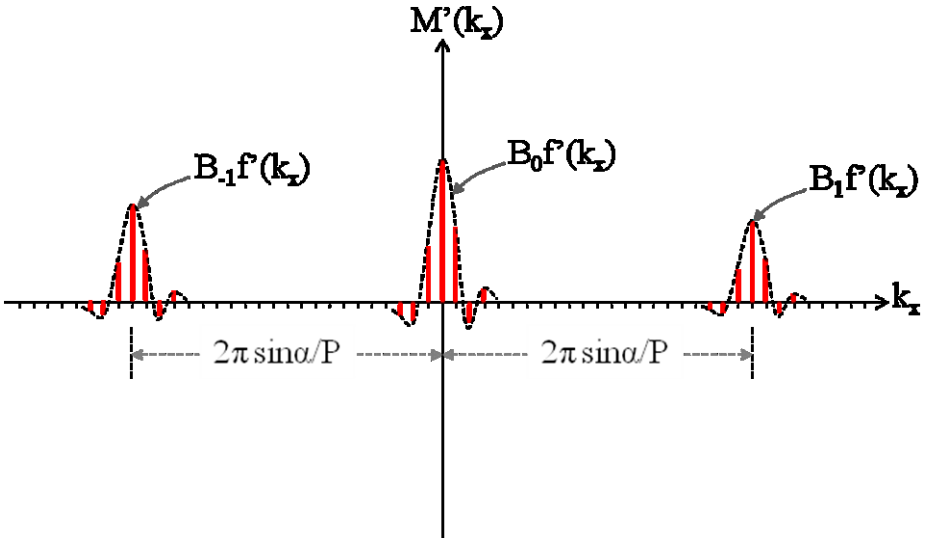

Figure 5. The Fourier transformation of the grating modulation function is non-zero at discrete steps of $2\pi/(H/\sin\alpha)$. It is a series of copies of the *f*' function at locations $2\pi m/(P/\sin\alpha)$.

The detector screen is set parallel to the grating back plane, at z = *L*. The wave on the detector screen is derived from Eq.(5) and (6) to be

$$A(x, z = L) = \sum_{m,n} B_m \exp(ik_{xn}x + ik_{zn}L) f'(\delta k_{nm}), \tag{7}$$

where

$$\begin{aligned} k_{xn} &= k_x + 2\pi m \sin\alpha / H, \\ k_{zn} &= \sqrt{k^2 - k_{xn}{}^2}, \end{aligned} \tag{8}$$

and

$$\delta k_{nm} = 2\pi m \sin\alpha / H - 2\pi m \sin\alpha / P. \tag{9}$$

We define

$$\begin{aligned} k_{mx} &= k_x + 2\pi m \sin\alpha / P, \\ k_{mz} &= \sqrt{k^2 - k_{mx}{}^2}. \end{aligned} \tag{10}$$

Then by Fresnel approximation

$$\begin{aligned} k_{xn} &= k_{mx} + \delta k_{nm}, \\ k_{zn} &\approx k_{mz} - \delta k_{nm} \cot(\alpha_m) - \delta k_{nm}{}^2 / (2k \sin^3 \alpha_m), \end{aligned} \tag{11}$$

where α_m is the mth order diffraction angle of an ideal infinite multilayer grating:

$$\alpha_m = \arccos(k_{mx} / k). \tag{12}$$

For tabletop devices running at 5 – 100 keV with P between 100 nm and 1000 nm, H ~ 10 μm and the distance between the grating and the detector less than 1 meter, the following approximations are valid:

$$\begin{aligned} &\cot(\alpha_m) \approx \cot(\alpha) + 2\pi m/(Pk\sin^2\alpha), \\ &\sin^3(\alpha_m) \approx \sin^3(\alpha). \end{aligned} \tag{13}$$

Substituting these approximations into Eq.(11) and the result into Eq.(7) yields

$$\begin{aligned} A(x, z = L) = \sum_m B_m \exp(ik_{mx}x + ik_{mz}L) \\ \sum_n f'(\delta k_{nm}) \exp[i\delta k_{nm}(x - m\Delta - L\cot\alpha) - iL\delta k_{nm}{}^2/(2k\sin^3\alpha)], \end{aligned} \tag{14}$$

where

$$\Delta = L\lambda/(P\sin^2\alpha). \tag{15}$$

In Eq.(14) the summation over n is recognized as the expression of a wave on the detector screen resulting from a plane wave incident on a virtual grating with a discrete Fourier spectrum

$$f_m'(k_x) = \sum_n f'(2\pi n\sin\alpha/H - 2\pi m\sin\alpha/P)\delta(k_x - 2\pi n\sin\alpha/H)\,. \tag{16}$$

Thus, the wave function on the detector screen can be expressed as

$$A(x, z = L) = \sum_m B_m \exp(ik_{mx}x + ik_{mz}L) S_m(x - m\Delta, z = L)\,, \tag{17}$$

where S_m is an envelope function equivalent to the diffracted wave by a virtual grating defined in Eq.(16). Equation (17) shows that the mth diffraction order of an infinite multilayer is now modulated by a substrate level wave function.

If we can precisely control the bilayer thickness such that the multilayers precisely fill the stair height, then H is an integer multiple of P, and the envelop function S_m is independent of the diffraction order m (Eq.(16)). Thus,

$$A(x, z = L) = \sum_m B_m \exp(ik_{mx}x + ik_{mz}L) S(x - m\Delta, z = L)\,, \tag{18}$$

where S is the common envelop function for all primary diffraction orders. Equation (18) shows that the diffracted wave of the grating array is that of an infinite grating multiplied by a substrate level envelope. The envelope is equivalent to the transmitted wave through a substrate grating, which is defined by the modulation $f(x)$ of each stair.

Ideally we would like to eliminate the substrate-level envelope modulation. Two necessary conditions to achieve this goal are 1. the continuity condition, where the multilayers precisely fill the height of the stairs and 2. the uniform phase shift condition, in which the linear phase ramp across each micro grating is removed. The latter can be realized by depositing a filler layer of silicon over the grating followed by polishing. In the resulting structure the penetration depth of Si is uniform over the entire grating.

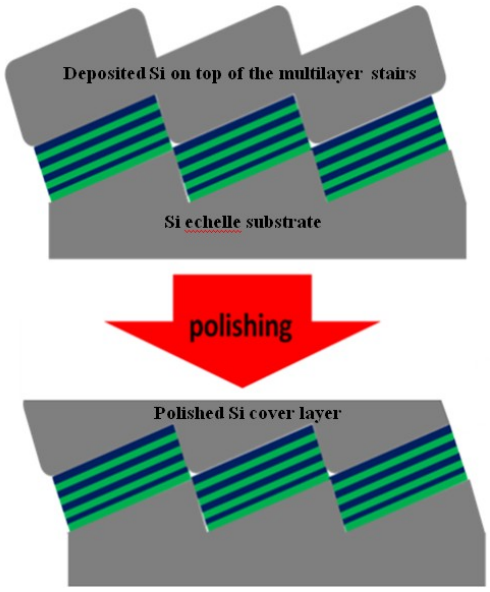

Figure 6. A filler layer of silicon is deposited on the top of the grating and polished to equalize x-ray penetration path lengths through the substrate.

3. GRATING ARRAY FABRICATION

3.1 Grating fabrication

Figure 3 illustrates the design of the grating substrate. The substrate is made by a photolithography procedure. First a nitride mask of 10 micron period is laid on the <100> wafer with the nitride strips aligned with the <111>surfaces. KOH etching of the wafer exposes the <111> surfaces. These are the floor and side walls of the stairs, and the angle between them is 70.53°. The resulting height of each stair is 8164.9 nm. The sharpness of the edge of the stairs is controlled by the width of the nitride mask strips and the amount of under-etch. Experimentally the edges were narrow plateaus of 1.0 microns for our substrates.

The substrate design is a balance between the blaze angle α in Fig. 4 and the Si wafer thickness, since the penetration depth of x-rays through the wafer is given by

$$D = t / \sin\alpha, \tag{19}$$

where t is the wafer thickness. A small blaze angle is advantageous from the multilayer deposition perspective, since less layers need to deposited and there will be less side wall deposition. However, smaller blaze angles lead to larger penetration depths through the wafer and more attenuation of transmitted intensity. In our first fabrication the blaze angle was set by the <100> orientation of the wafer surface to 54.7°. The wafer was placed in a magnetron sputtering chamber at 35° angle from the usual horizontal plane. The purpose of the tilt was to reduce deposition on the side walls of the stairs. Silicon and tungsten layers were alternately deposited onto the substrate with dual source configuration of the chamber. A total of 20 layers (10 bilayers) were deposited over a period of 26 hours.

3.2 Surface inspection of multilayer adhesion to substrate

The W/Si bilayers are known to have tensile stresses, so adhesion to the substrate was a concern. We inspected the coated surfaces of the Si wafers with optical and scanning electron microscopy (SEM). There was no detachment or delamination in the etched grating area or at cleaved edges of the grating (Fig.7a). Detachment occurred at the fringe of

the un-patterned flat areas of the wafer (Fig.7b). It seems that the staircase surface improved the adhesion of the multilayer to the Si substrate.

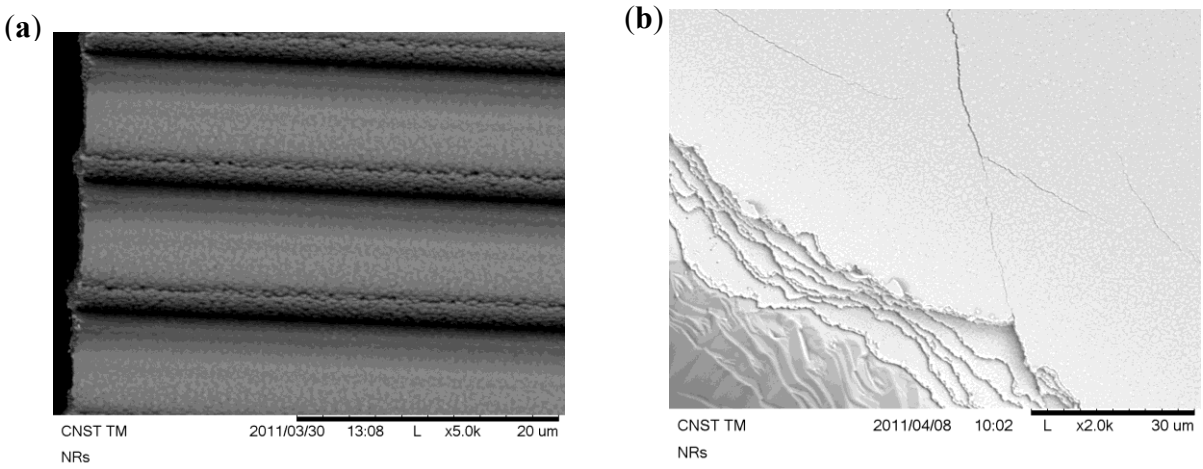

Figure 7. (a) Top-down SEM of the cleaved edge of multilayer coated grating area shows no detachment of the layers. The ridges are the coated stairs of the substrate. Referring to Fig.3, the smooth side of the ridge is the floor surface of the stair. The rough side of the ridge is the side wall of the stair. Substantial coating on the side wall can be seen. (b) Top-down SEM of the flat area of the wafer shows occasional cracks and delamination, possibly due to the tensile stress of the W/Si multilayer.

3.3 Cross-section inspection

The coated wafers were cleaved along the <110> direction and inspected by SEM. No polishing was applied. Figure 8 shows the cross section profiles at low magnification on the left and high magnification on the right. The multilayer on the flat part of the wafer amounted to a total thickness of 7.21 µm. The layers on the grating area are well defined and the tungsten layers are thicker than the silicon layers. There was substantial deposition on the side wall of the stairs. Both the floor and side wall multilayers taper down slightly towards the corner of the stairs. The total thickness of deposition on the floor surface was 5.5 µm on average, and on the side wall was 4.2 µm on average.

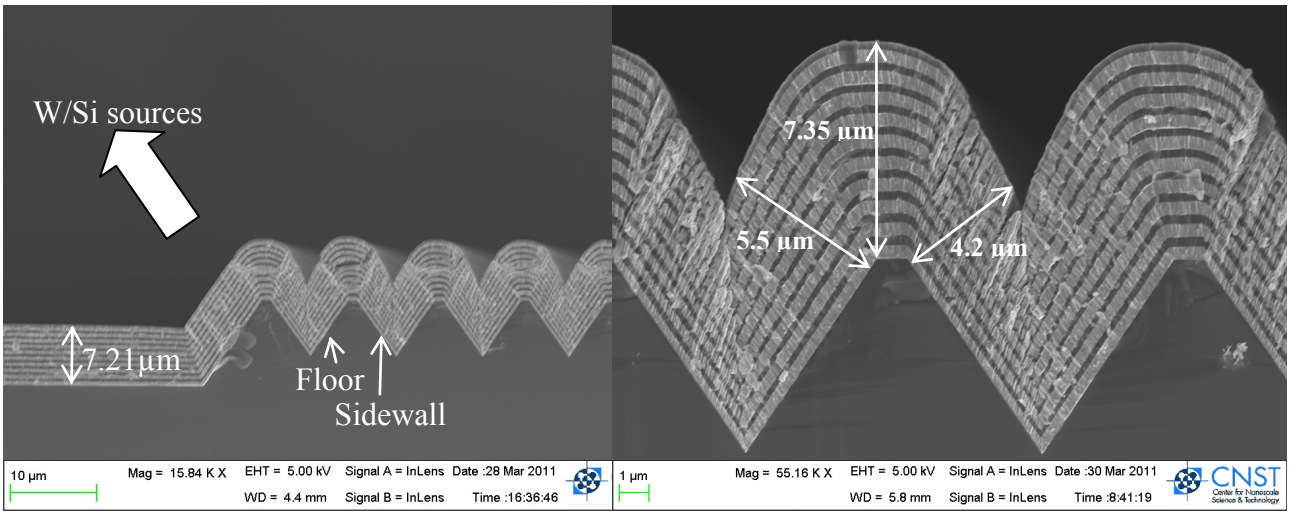

Figure 8. Cross section electron micrographs of the multilayer coated staircase substrate. The darker layers are silicon.

4. CONCLUSION

In order to improve the sensitivity of hard x-ray grating interferometers and overcome the aspect ratio limitation of grating periods, we propose a multilayer micro grating array in the transmission geometry using a staircase substrate. The idea is inspired by EUV multilayer blazed reflection gratings. Theoretical modeling points to two necessary conditions to achieve continuity between the micro gratings: control of the bilayer thickness to an integer fraction of the stair height, and a top substrate filler layer to equalize the transmission path lengths. In our first fabrication tests using magnetron sputtering of W/Si bilayers, we found uniform adhesion of the multilayer to the substrate throughout the grating area, and multilayer structure of good integrity on the floor surface. On the other hand, there was substantial deposition on the side walls of the stairs and the layer thicknesses were tapered towards the corner of the stairs. The same backside deposition was also seen in EUV blazed gratings. Based on these findings, we plan to reduce the blaze angle from the current 54.7° to between 20° to 30°. Although a smaller blaze angle means a thinner substrate is necessary, the advantage may be less side wall deposition and better control of the bilayer thickness. Alternatively, electron beam vacuum deposition may also be considered as a way to improve directionality of the deposition beam, and thereby reducing side wall deposition.

REFERENCES

[1] Yokozeki S.and Suzuki T., "Shearing Interferometer Using Grating as Beam Splitter," Applied Optics 10(7), 1575-1580 (1971).

[2] David C., Nohammer B., Solak H. H.and Ziegler E., "Differential x-ray phase contrast imaging using a shearing interferometer," Applied Physics Letters 81(17), 3287-3289 (2002).

[3] Momose A., Kawamoto S., Koyama I., Hamaishi Y., Takai K.and Suzuki Y., "Demonstration of X-Ray Talbot interferometry," Japanese Journal of Applied Physics Part 2-Letters 42(7B), L866-L868 (2003).

[4] Weitkamp T., Diaz A., David C., Pfeiffer F., Stampanoni M., Cloetens P.and Ziegler E., "X-ray phase imaging with a grating interferometer," Optics Express 13(16), 6296-6304 (2005).

[5] Takeda Y., Yashiro W., Suzuki Y., Aoki S., Hattori T.and Momose A., "X-ray phase imaging with single phase grating," Japanese Journal of Applied Physics Part 2-Letters & Express Letters 46(1-3), L89-L91 (2007).

[6] Pfeiffer F., Bech M., Bunk O., Kraft P., Eikenberry E. F., Bronnimann C., Grunzweig C.and David C., "Hard-X-ray dark-field imaging using a grating interferometer," Nature Materials 7(2), 134-137 (2008).

[7] Wen H., Bennett E., Hegedus M. M.and Carroll S. C., "Spatial harmonic imaging of x-ray scattering - initial results," IEEE Transactions on Medical Imaging 27(8), 997-1002 (2008).

[8] Wang Z. T., Kang K. J., Huang Z. F.and Chen Z. Q., "Quantitative grating-based x-ray dark-field computed tomography," Applied Physics Letters 95(9), (2009).

[9] Wernick M. N., Wirjadi O., Chapman D., Zhong Z., Galatsanos N. P., Yang Y. Y., Brankov J. G., Oltulu O., Anastasio M. A.and Muehleman C., "Multiple-image radiography," Physics in Medicine and Biology 48(23), 3875-3895 (2003).

[10] Davis T. J., "A unified treatment of small-angle x-ray-scattering, x-ray refraction and absorption using the Rytov approximation," Acta Crystallographica Section A, 50 686-690 (1994).

[11] David C., Bruder J., Rohbeck T., Grunzweig C., Kottler C., Diaz A., Bunk O.and Pfeiffer F., "Fabrication of diffraction gratings for hard X-ray phase contrast imaging," Microelectronic Engineering 84(5-8), 1172-1177 (2007).

[12] Noda D., Tanaka M., Shimada K., Yashiro W., Momose A.and Hattori T., "Fabrication of large area diffraction grating using LIGA process," Microsystem Technologies-Micro-and Nanosystems-Information Storage and Processing Systems 14(9-11), 1311-1315 (2008).

[13] Liu C., Conley R., Macrander A. T., Maser J., Kang H. C., Zurbuchen M. A.and Stephenson G. B., "Depth-graded multilayers for application in transmission geometry as linear zone plates," Journal of Applied Physics 98(11), 113519 (2005).

[14] Kang H. C., Maser J., Stephenson G. B., Liu C., Conley R., Macrander A. T.and Vogt S., "Nanometer linear focusing of hard x rays by a multilayer Laue lens," Physical Review Letters 96(12), (2006).

[15] Kim J. M., Cho I. H., Lee S. Y., Kang H. C., Conley R., Liu C. A., Macrander A. T.and Noh D. Y., "Observation of the Talbot effect using broadband hard x-ray beam," Optics Express 18(24), 24975-24982 (2010).

[16] Voronov D. L., Ahn M., Anderson E. H., Cambie R., Chang C. H., Gullikson E. M., Heilmann R. K., Salmassi F., Schattenburg M. L., Warwick T., Yashchuk V. V., Zipp L.and Padmore H. A., "High-efficiency 5000 lines/mm multilayer-coated blazed grating for extreme ultraviolet wavelengths," Optics Letters 35(15), 2615-2617 (2010).